European Journal of Mechanics / A Solids 109 (2025) 105453

Contents lists available at ScienceDirect

European Journal of Mechanics / A Solids

journal homepage: www.elsevier.com/locate/ejmsol

Full Length Article

Combined extension and torsion of hydrogels with chemo-mechanical coupling: Revealing positive poynting effect

Chengxiang Zheng [a,b], Minghui Hu [a,b], Wenyi Wang [a,b], Qian Li [d,e,*], Pasquale Ciarletta [c], Tao Wu [a,b,**], Zichen Deng [a,b,***]

[a] School of Mechanics, Civil Engineering and Architecture, Northwestern Polytechnical University, Xi'an, 710072, China
[b] MIIT Key Laboratory of Dynamics and Control of Complex Systems, Xi'an, 710072, China
[c] MOX, Dipartimento di Matematica, Politecnico di Milano, piazza Leonardo da Vinci 32, 20133, Milan, Italy
[d] China Electronic Product Reliability and Environmental Testing Research Institute, China
[e] Guangdong Provincial Key Laboratory of Electronic Information Products Reliability Technology, China

ARTICLE INFO

Keywords:
Extension and torsion
Hydrogel
Chemo-mechanical coupling
Continuum mechanical framework
Positive poynting effect

ABSTRACT

In this paper, combined extension and torsion of hydrogel subject to a chemo-mechanical coupled loading is described in the framework of continuum mechanics, where the free energy density consists of the elastic, mixing and chemical contributions. A simplified, closed-form and exactly analytical solution to the mechanical response is obtained, which accounts for the coupling effect of external loading, chemical potential and microstructural parameters, such as crosslinking degree, Flory-Huggins parameter, etc. In particular, the effect of free swelling and microscopic diffusion on deformation of the hydrogel at equilibrium state is discussed, reaching some fundamental conclusions. Negative axial forces are captured, revealing the typical positive Poynting effect where the cylinder tends to elongate on twisting, and an inhomogeneous deformation, induced by torsion, along the radial direction is demonstrated. Furthermore, the dynamic competition between external loading and solvent environment is revealed and investigated, where the direct connection between internal micro-physical parameters and macroscopic deformation is demonstrated. The theoretical results presented in this paper may provide predictions and guidance for the mechanical analysis and design of hydrogel cylinder subject to extension and torsion in a solvent.

1. Introduction

Hydrogels are a fascinating group of polymers characterized by their unique three-dimensional network structure, established through chemical or physical cross-linking. From a macroscopic point of view, hydrogels deform quasi-elastically in such a way that they change volumes and shapes when external mechanical or chemical loading is applied and gradually return to the original after the loading is removed. On a microscopic scale, the presence of a porous network structure enables water-soluble small molecules to diffuse into or out of the gel, with a diffusion coefficient comparable to that in aqueous solutions, indicating liquid-like properties. As a result, hydrogels exhibit both solid and liquid properties, making them highly versatile and valuable in various applications (Hao et al., 2022; Li et al., 2021, 2023). Furthermore, film-substrate systems made with hydrogels are widely used in flexible electronic devices, and the buckling behaviour subject to different external loads is discussed (Liu et al., 2022; Su et al., 2018; Wang et al., 2020). Therefore, the understanding of the physical mechanisms that link the macroscopic mechanical deformations of hydrogels to the microstructure and solvent environment is an important foundation for its design and application.

The nonlinear phenomenon that a cylinder tends to elongate under simple torsion was first experimentally discovered by and named after Poynting, as Poynting effect, on steel, copper and brass wires (Poynting, 1909, 1912). Afterwards, torsion of solid cylinder has been widely investigated for different types of loads and boundaries, and for variant materials, such allies and polymeric materials with series of constitutive relations. Rivlin exploited a neo-Hookean model to calculate the forces

* Corresponding author.
** Corresponding author. School of Mechanics, Civil Engineering and Architecture, Northwestern Polytechnical University, Xi'an, 710072, China.
*** Corresponding author. School of Mechanics, Civil Engineering and Architecture, Northwestern Polytechnical University, Xi'an, 710072, China.
E-mail addresses: liqian.1234@163.com (Q. Li), wut@nwpu.edu.cn (T. Wu), dweifan@nwpu.edu.cn (Z. Deng).

https://doi.org/10.1016/j.euromechsol.2024.105453
Received 29 April 2024; Received in revised form 6 September 2024; Accepted 17 September 2024
Available online 19 September 2024

required to produce certain simple types of deformation in a uniform tube of circular cross-section with simultaneous extension, inflation and torsion, where the strain energy density is linearly dependent on the first strain invariant (Rivlin, 1949). This model was then modified with a Mooney-Rivlin model to analysis the nonlinear deformation of rubbery elastomer, where an additive linear component of the second invariant is included (Ogden, 1997). Later, Horgan et al. discussed positive/-negative Poynting effect, that the cylinder tends to elongate or shorten on twisting, through investigation into finite deformation of soft rubber-like cylinder subject to variant loadings such as simple torsion and torsion with extension (Horgan and Murphy, 2015; Kanner and Horgan, 2008a, 2008b). Subsequently, equi-biaxial extension, simple shear and pure torsion were also analyzed for soft biomaterials based on FD-model, further confirming the importance of the second strain invariant in constitutive models (Demiray, 1972; Fung, 1967; Horgan and Smayda, 2012). Recently, the finite extension and torsion of an elastic circular of isotropic nonlinear elastic solid is described with the Blatz-Ko constitutive models (Kirkinis and Ogden, 2016; Polignone and Horgan, 1991). However, in the study of fluid-infused materials, such as hydrogels and biological tissues, solvent diffusion and large volume change can occur and the effect of chemical potential becomes significant (Horgan and Murphy, 2015). A second-order nonlinear elastic theory with chemical coupling for biogels is proposed by Wu et al., through perturbation analysis on the basis of statistical mechanics constitutive formulation (Wu and Kirchner, 2010). Afterwards, the simple shear and torsion with axial loading of bilayer composite biogels were investigated to reveal the Poynting effect (Wang and Wu, 2014; Wu and Wang, 2015). Although the aforementioned models proved capable of phenomenally simulating the complex deformation, the underling mechanism and microscopic association with macroscopic behavior are still not well understood.

From the framework of thermodynamics and continuum mechanics, a series of multiphysics field models have been proposed for hydrogels recently, and the shortcomings of the nonlinear elasticity model of extension and torsion can be well overcome. Motivated by the experimental observation, Dolbow et al. developed a continuum model for chemically induced volume phase transition in hydrogels, in which the coupling between the deformation and solute concentration is formulated through the interfacial normal conjugational force balance (Dolbow et al., 2004; Ji et al., 2006). Hong et al. proposed a non-equilibrium coupled model of molecular migration and large deformations, where the free energy is derived from stretching the network and mixing the network with small molecules (Hong et al., 2008, 2009), and remote migration is successfully modelled via coupling diffusion of small molecules with the overall deformation of hydrogel. Furthermore, Li et al. proposed a multi-effect-coupling thermal-stimulus (MECtherm) model to simulate the responsive behavior of hydrogels due to multi-physical coupled stimuli (Li et al., 2005, 2007, 2009). Similar work was conducted by Chester et al. (Chester and Anand, 2010) and Duda et al., 2010, 2018 by introducing a multiplicative decomposition of the deformation gradient. Based on the constitutive models formulated by statistically mechanics principles, those models have depicted a comprehensive description of both macro and microscopic properties of hydrogel. In analytical practices, however, the inhomogeneous deformation and the coupling between extension and torsion, induced by the twisting of hydrogels, remain unclear. Therefore, it is still a pressing and advanced issue to investigate the extension and torsion of hydrogel cylinder along with the dynamic diffusion of solvent molecules, and the influence of the chemical potential on nonlinear deformations.

Consequently, in this paper, the extension and torsion of hydrogel cylinder subject to a chemo-mechanical coupled field is analyzed in the framework of continuum mechanics, where a statistical formulation of free energy density is adopted, consisting of the elastic, mixing and chemical contributions. As a result, a simplified, closed-form and exactly analytical solution of the mechanical response is obtained, which couples the effect of chemical potential and microstructure material parameters, such as crosslinking degree, Flory-Huggins parameter, etc. In particular, the dynamic competition between mechanical and chemical loading is revealed and discussed, and the direct connection between internal micro-physical parameters and macroscopic deformation is demonstrated.

This paper is organized as follows. First in Section 2, the extension and torsion of hydrogel cylinder subject to chemo-mechanical coupled field is analytically investigated in the framework of continuum mechanics, including isotropic free swelling. Then in Section 3, the effects of Flory-Huggins parameter and degree of crosslinking are theoretically analyzed on the torque and axial force on the surface of a cylindrical, where all the results are dependent on the chemical potential. In addition, the classic nonlinear positive Poynting effect is reveled where the cylinder tends to elongate on twisting. A summary of this paper and conclusions are given in the last section.

2. Formulation

In this section, the extension and torsion of hydrogel cylinder with chemical coupling is formulated in the framework of continuum mechanics. It should be noted that the hydrogel remains in a state of equilibrium within the solvent, where the amounts of solvent moving in and out of the hydrogel are dynamically balanced. The transient diffusion process over time, however, is not considered in this context.

As illustrated in Fig. 1, the upper and lower end faces of the hydrogel specimen is twisted by parallel circular plates, and the deforming process may be decomposed into two steps in this study. Firstly, the cylinder specimen at dry state with radius R_0 and height H isotropically swells to a stretch λ_0, depicting an interstitial state with radius $r_0 = \lambda_0 R_0$ and height $h = \lambda_0 H$. Then a torque T_0, along with an axial load F, is imposed on the top surface to induce a rotation of the upper plane $z = h$ to an angle $\varphi = \frac{\gamma}{r} \cdot h$ with respect to the fixed bottom plane surface $z = 0$, while the axial stretch λ_0 remains unchanged. It is noted that the chemical equilibrium is broken by torsion along the radial direction, to maintain the radial force balance. As a result, solvent molecules might migrate radially due to the gradient of chemical potential, and finally reach an equilibrium with inhomogeneous deformation. Alongside, an axial loading F is required to maintain the stretch, as a result of nonlinear effect.

Following the classical theoretical framework of nonlinear continuum mechanics, the description of deformations can be defined as a mapping ψ: $\Omega_0 \rightarrow \Omega$, from reference configuration Ω_0 to the current configuration Ω at time t. The deformation gradient $\boldsymbol{F} = \mathrm{Grad}\boldsymbol{x} = d\boldsymbol{x}/d\boldsymbol{X}$ then describes the deformation kinematics from a reference point $\boldsymbol{X} \in \Omega_0$ to its current position $\boldsymbol{x} = \psi(\boldsymbol{X}, t) \in \Omega$ in the configuration Ω at time t. Typically, hydrogel is considered as a condensed matter with negligible void space, and the volume change of the hydrogel is achieved by absorbing and discarding solvents. Subsequently, the molecular incompressibility condition is expressed as (Hong et al., 2008)

$$1 + vC = J = \det \boldsymbol{F} \tag{1}$$

where v is the volume per solvent molecule, C is the number of the solvent molecules per unit volume inside the hydrogel, and J is the determinant of the deformation gradient $\boldsymbol{F}$.

2.1. Isotropic swelling

When the hydrogel specimen is immersed in solvent in the absence of any external force, it may deform from the initial state (a) to the interstitial swelling state (b), as shown in Fig. 1. A swelling equilibrium is achieved when the two opposite tendencies cancel each other out, that is, the volume expansion caused by solvent penetration and the elastic contraction generated by the internal network structure. A material point $\boldsymbol{X} = X_i \boldsymbol{E}_i$ then moves to a place with coordinate $\boldsymbol{x}'$ in the interstitial frame that is equilibrated with the surrounding chemical potential μ_0,

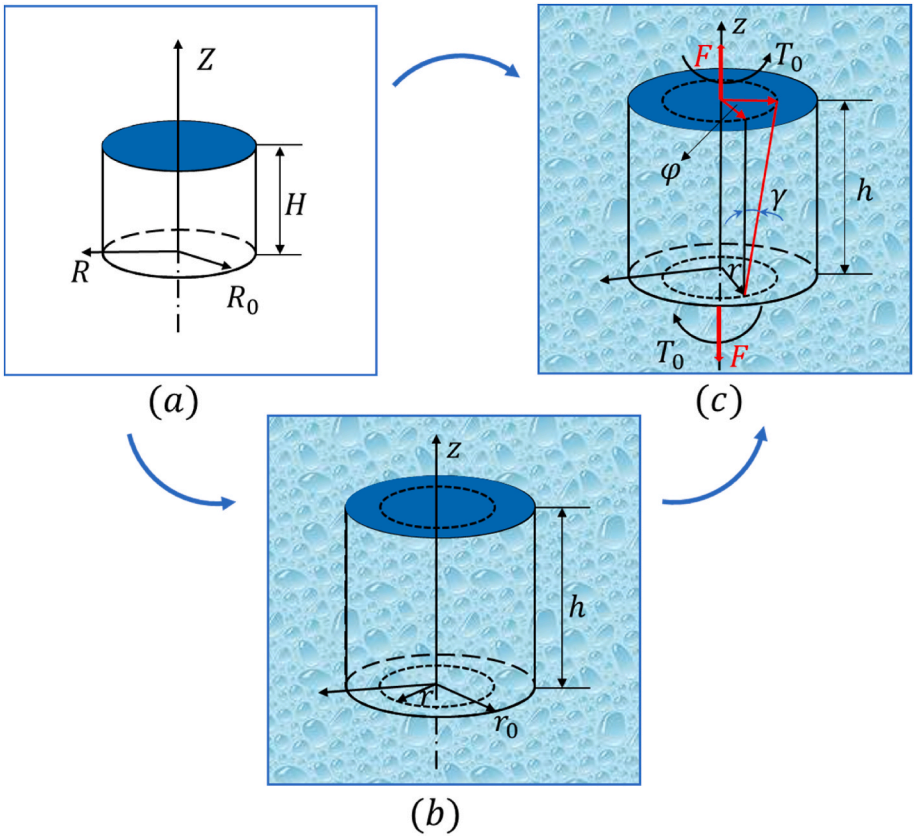

Fig. 1. Schematic of soft cylinder subject to torsion in solvent. Initially, a hydrogel cylinder is at reference state (dry state) with radius R_0 and length H (a). It is then immersed in solvent and swells isotopically to an interstitial state with a stretch λ_0 (free swelling state) with radius $r_0 = \lambda_0 R_0$ and length $h = \lambda_0 H$ (b). Extension and torsion of the swollen cylinder in a solvent to an angle $\varphi = \frac{\gamma}{r} \cdot h$ subject to torque T_0 and an axial load F, and invariant axial stretch λ_0 subject to axial load F, where the plane surface $z = 0$ remains fixed (c).

and the coordinate $\boldsymbol{x}'$ is obtained as

$$\boldsymbol{x}' = x_{1'}\boldsymbol{e}_{1'} + x_{2'}\boldsymbol{e}_{2'} + x_{3'}\boldsymbol{e}_{3'} = \lambda_0 X_1 \boldsymbol{e}_{1'} + \lambda_0 X_2 \boldsymbol{e}_{2'} + \lambda_0 X_3 \boldsymbol{e}_{3'} \tag{2}$$

or in polar system as $\boldsymbol{x}' = r'\boldsymbol{e}_{r'} + z'\boldsymbol{e}_{z'}$, where the interstitial radial, angular, and axial coordinate (r', θ', z') is associated with those in the reference state (R, Θ, Z) as

$$r' = \lambda_0 R$$

$$\theta' = \Theta$$

$$z' = \lambda_0 Z \tag{3}$$

Since the specimen undergoes an isotropic swelling, the interstitial base vectors $\boldsymbol{e}_{i'}$ are identical to those in the reference state $\boldsymbol{E}_K$, i.e. $\boldsymbol{e}_{r'} = \boldsymbol{E}_R, \boldsymbol{e}_{\theta'} = \boldsymbol{E}_\Theta, \boldsymbol{e}_{z'} = \boldsymbol{E}_Z$. Given that the only non-trivial derivatives of base vectors is $\frac{\partial \boldsymbol{E}_\Theta}{\partial \Theta} = \boldsymbol{E}_R$, the isotropic deformation gradient $\boldsymbol{F}_0$ is thus given as (Hong et al., 2009)

$$\boldsymbol{F}_0 = \mathrm{Grad}\boldsymbol{x}' = \frac{\partial \boldsymbol{x}'}{\partial \boldsymbol{X}} = \boldsymbol{x}' \otimes \left(\boldsymbol{E}_R \frac{\partial}{\partial R} + \boldsymbol{E}_\Theta \frac{1}{R} \frac{\partial}{\partial \Theta} + \boldsymbol{E}_Z \frac{\partial}{\partial Z} \right) = \begin{bmatrix} \lambda_0 & 0 & 0 \\ 0 & \lambda_0 & 0 \\ 0 & 0 & \lambda_0 \end{bmatrix} \tag{4}$$

where $\mathrm{Grad}(\cdot) = \frac{\partial (\cdot)}{\partial \boldsymbol{X}} = (\cdot) \otimes \left(\boldsymbol{E}_R \frac{\partial}{\partial R} + \boldsymbol{E}_\Theta \frac{1}{R} \frac{\partial}{\partial \Theta} + \boldsymbol{E}_Z \frac{\partial}{\partial Z} \right)$ denotes the right gradient of a variable $(\cdot)$ with respect to the reference frame $\boldsymbol{X}$ in a cylindrical coordinate system, and the volume ratio J is the determinant of deformation gradient $\boldsymbol{F}_0$, namely $J = \det \boldsymbol{F}_0 = \lambda_0^3$.

Furthermore, the first Piola-Kirchhoff (PK1) stress $\boldsymbol{P}$ is work-conjugate with the deformation gradient $\boldsymbol{F}$, and it can be given as

$$\boldsymbol{P} = \frac{\partial \widehat{W}}{\partial \boldsymbol{F}} \tag{5}$$

where $\widehat{W}$ is the free energy density of hydrogels. Consequently, the true stress $\boldsymbol{\sigma}$ is hence formulated as

$$\boldsymbol{\sigma} = \frac{1}{J} \boldsymbol{P} \boldsymbol{F}^T = \frac{1}{J} \frac{\partial \widehat{W}}{\partial \boldsymbol{F}} \boldsymbol{F}^T \tag{6}$$

If no body force is considered, the balance of force, in terms of the true stress $\boldsymbol{\sigma}$, is then formulated as

$$\boldsymbol{\sigma} \cdot \nabla = \boldsymbol{0} \tag{7}$$

Constitutively, the total free energy density $\widehat{W}$ of hydrogels, generally depending on the deformation $\boldsymbol{F}$ and concentration C, contains contributions form stretching the network $W_e(\boldsymbol{F})$ and mixing the polymer and solvent $W_m(C)$. While the chemical field may be coupled through Legendre transformation, resulting in a new form of free energy density $W(\boldsymbol{F}, \mu)$, depending on the deformation $\boldsymbol{F}$ and chemical potential of the interstitial solvent μ, as (Wu et al., 2022; Zheng et al., 2022)

$$W(\boldsymbol{F}, \mu) = \widehat{W} - \mu C \tag{8}$$

Following the Flory-Rehner model, the stretching energy density W_e of the hydrogel network is (Flory and Rehner, 1943)

$$W_e(\boldsymbol{F}) = \frac{NkT}{2} (\boldsymbol{F} : \boldsymbol{F} - 3 - 2 \ln J) \tag{9}$$

where N is the number density of polymer chains, k is the Boltzmann constant, T is the temperature.

And the free energy density of mixing the polymer and solvent W_m (Hong et al., 2008; Huggins, 1941), can be given as

$$W_m(C) = -\frac{kT}{v}\left[vC\ln\left(1+\frac{1}{vC}\right)+\frac{\chi}{1+vC}\right] \tag{10}$$

where χ is the Flory-Huggins parameter.

Upon substituting Eqs (1), (9) and (10) into Eq. (8), the total free energy density W can then be explicitly expressed as below.

$$W(\boldsymbol{F},\mu) = \frac{NkT}{2}(\boldsymbol{F}:\boldsymbol{F}-3-2\ln J) - \frac{kT}{v}\left[(J-1)\ln\frac{J}{J-1}+\frac{\chi}{J}\right] - \mu\frac{(J-1)}{v} \tag{11}$$

Consequently, by Eqs (4) and (11), and setting stress (6) to zero, namely $\boldsymbol{\sigma} = \mathbf{0}$, the relationship between chemical potential μ_0 and stretching λ_0 for free swelling can then be obtained as

$$\frac{1}{\lambda_0} = \frac{1}{vN}\left[\frac{\mu_0}{kT} - \ln\left(1-\frac{1}{\lambda_0^3}\right) - \frac{1}{\lambda_0^3} - \frac{\chi}{\lambda_0^6}\right] + \frac{1}{\lambda_0^3} \tag{12}$$

It should be noted that the chemical potential μ_0 at the equilibrium steady state is non-dimensionalized with kT, that is $\tilde{\mu} = \mu_0/kT$. As a result, Eq. (12) is normalized with only two dimensionless material parameters, vN and χ, to formulate the chemo-mechanical coupling constitutive relation of the hydrogel at the equilibrium state. Subsequently, the isotropic swelling ratio λ_0 of the hydrogel is discussed in details for the influence of the non-dimensionalized chemical potential $\tilde{\mu}$, the crosslinking vN and the Flory-Huggins parameter χ. By Eq. (12), Fig. 2 shows the variation of the stretch λ_0 with (a) the non-dimensionalized chemical potential $\tilde{\mu} = \mu_0/kT$ with $\chi = 0.2$ and $vN = 10^{-3}$, (b) the Flory-Huggins parameter χ with $\tilde{\mu} = -10^{-3}$ and $vN = 10^{-3}$, and (c) the crosslinking vN with $\chi = 0.2$ and $\tilde{\mu} = 10^{-3}$, respectively. Here, a representative value of the volume per molecule is set as $v = 10^{-28}m^3$, the range of crosslinking is $vN = 10^{-4} \sim 10^{-1}$, and $kT = 4\times10^{-21}J$ at room temperature in this paper. Combining Fig. 2 and Eq. (12), the following properties are found.

a) It is demonstrated that the stretch λ_0 increases with larger chemical potential $\tilde{\mu}$, and that the stretch λ_0 approaches 1 corresponding to the initial dry gel state when the chemical potential $\tilde{\mu}$ approaches negative infinity, meaning no solvent is inside the hydrogel network.
b) The parameter χ serves as a dimensional measure of the enthalpy of mixing, indicating the hydrophobicity of hydrogel. In applications where gels with significant swelling ratios are desired, materials possessing low χ values are typically utilized.
c) With the increase of the internal structural parameter crosslinking vN, the material becomes stiffer, leading to a gradual decrease in the corresponding macroscopic elongation.

Furthermore, all of the curves in Fig. 2 exhibit monotonicity when using the chemical formula as the independent variable. With the free swelling study and discussion in this subsection, the above summary will play an essential and fundamental role in the ensuing analyses and investigation.

2.2. *Chemically coupled extension and torsion: Poynting effect and radial inhomogeneity*

After the first step of swelling, a combined torque T_0 and axial loading F is then imposed on the top surface of the hydrogel cylinder, with bottom surface fixed, to induce a rotation of the upper plane, along with an unchanged stretch λ_0, where the deformation process is assumed always in solvent and at equilibrium state. Subsequently, the final coordinate $\boldsymbol{x} = r\boldsymbol{e}_r + z\boldsymbol{e}_z$ is obtained as (Kirkinis and Ogden, 2016; Polignone and Horgan, 1991),

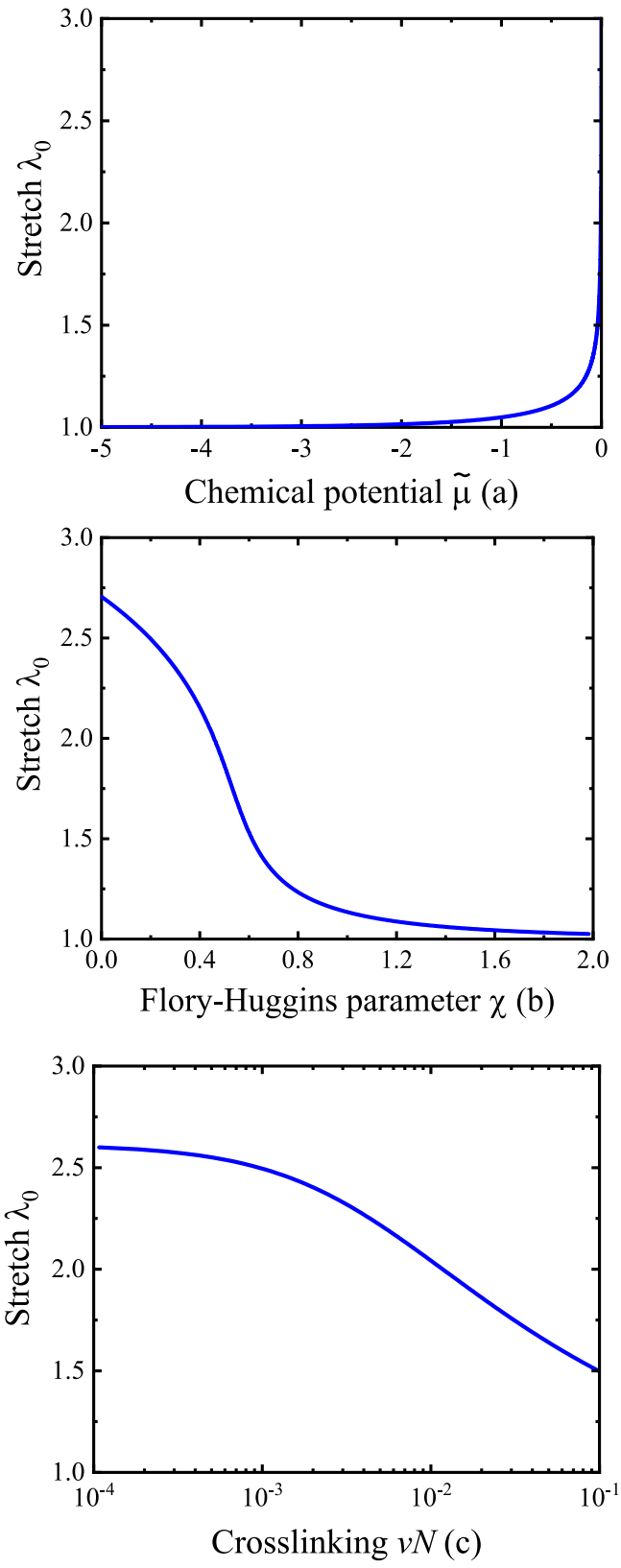

Fig. 2. Variation of the stretch λ_0 with different physical parameters subject to zero stress.

$$r = r' = r(R)$$

$$\theta = \theta' + \frac{\gamma}{r_0} z' = \Theta + \frac{\gamma}{r_0}\lambda_0 Z = \Theta + \zeta\lambda_0 Z$$

$$z = \lambda_z z' = \lambda_0 Z \tag{13}$$

Here, γ represents the twist per unit length of the deformed cylinder on the radial surface, $r_0 = \lambda_0 R_0$ is the radius of cylinder after swelling, the strain $\zeta = \frac{\gamma}{r_0}$ is the twist per unit length, and the final radial coordinate r varies with the reference position R, and we will denote $\dot{r} = \frac{dr}{dR}$ as its derivative with respect to R later in this paper.

In the context of infinitesimal deformation, the radial direction deformation (13) is homogeneous for an incompressible isotropic material, where the solution to pure torsion has been showed by Rivlin as $r = r' = \lambda_0 R$ (Rivlin and Rideal, 1948). In this case with finite deformation, however, the homogeneous radial deformation is no longer preserved due to the chemo-mechanical coupling and nonlinearity in constitutive relations. It is considered that the current radial coordinate r is no longer linearly associated with the reference position R, but as a function left to determine. As a consequence, the deformation gradient $\boldsymbol{F}$ is given by Eq. (13) as

$$\begin{aligned}\boldsymbol{F} &= \mathrm{Grad}\boldsymbol{x} = \boldsymbol{x} \otimes \left(\boldsymbol{E}_R \frac{\partial}{\partial R} + \boldsymbol{E}_\Theta \frac{1}{R}\frac{\partial}{\partial \Theta} + \boldsymbol{E}_Z \frac{\partial}{\partial Z}\right) \\ &= \dot{r}\boldsymbol{e}_r \otimes \boldsymbol{E}_R + \frac{r}{R}\boldsymbol{e}_\theta \otimes \boldsymbol{E}_\Theta + (\zeta r \lambda_0 \boldsymbol{e}_\theta + \lambda_0 \boldsymbol{e}_z) \otimes \boldsymbol{E}_Z\end{aligned} \tag{14}$$

And the three principal invariants of the deformation gradient $\boldsymbol{F}$ are

$$I_1 = \dot{r} + \frac{r}{R} + \lambda_0, I_2 = \frac{1}{2}\left(\frac{r\dot{r}}{R} + \dot{r}\lambda_0 + \frac{r\lambda_0}{R} - \zeta^2 r^2 \lambda_0^2\right), J = \frac{r\dot{r}}{R}\lambda_0 \tag{15}$$

The PK1 stress $\boldsymbol{P}$ is obtained by Eqs (5), (11) and (14), as

$$\boldsymbol{P} = \frac{\partial W(\boldsymbol{F}, \mu)}{\partial \boldsymbol{F}} = NkT(\boldsymbol{F} - \boldsymbol{F}^{-T}) + \frac{kT}{v}\left[\ln\left(1 - \frac{1}{J}\right) + \frac{1}{J} + \frac{\chi}{J^2} - \frac{\mu}{kT}\right] J\boldsymbol{F}^{-T} \tag{16}$$

Consequently, the true stress $\boldsymbol{\sigma}$ can be given as

$$\boldsymbol{\sigma} = \frac{1}{J}\boldsymbol{P}\boldsymbol{F}^T = \frac{NkT}{J}(\boldsymbol{F}\boldsymbol{F}^T - \boldsymbol{I}) + \frac{kT}{v}\left[\ln\left(1 - \frac{1}{J}\right) + \frac{1}{J} + \frac{\chi}{J^2} - \frac{\mu}{kT}\right]\boldsymbol{I} \tag{17}$$

or in matrix form as

$$\begin{aligned}\boldsymbol{\sigma} = \frac{1}{J}\boldsymbol{P}\boldsymbol{F}^T = \frac{NkT}{J}&\begin{bmatrix} \dot{r}^2 - 1 & 0 & 0 \\ 0 & (r/R)^2 + \lambda_0^2\zeta^2 r^2 - 1 & \lambda_0^2 \zeta r \\ 0 & \lambda_0^2 \zeta r & \lambda_0^2 - 1 \end{bmatrix} \\ &+ \frac{kT}{v}\left[\ln\left(1 - \frac{1}{J}\right) + \frac{1}{J} + \frac{\chi}{J^2} - \frac{\mu}{kT}\right]\boldsymbol{I}\end{aligned} \tag{18}$$

whose components are in the form of

$$\sigma_{rr} = \frac{NkT}{J}(\dot{r}^2 - 1) + \frac{kT}{v}\left[\ln\left(1 - \frac{1}{J}\right) + \frac{1}{J} + \frac{\chi}{J^2} - \frac{\mu}{kT}\right]$$

$$\sigma_{\theta\theta} = \frac{NkT}{J}\left[(r/R)^2 + \lambda_0^2\zeta^2 r^2 - 1\right] + \frac{kT}{v}\left[\ln\left(1 - \frac{1}{J}\right) + \frac{1}{J} + \frac{\chi}{J^2} - \frac{\mu}{kT}\right]$$

$$\sigma_{zz} = \frac{NkT}{J}(\lambda_0^2 - 1) + \frac{kT}{v}\left[\ln\left(1 - \frac{1}{J}\right) + \frac{1}{J} + \frac{\chi}{J^2} - \frac{\mu}{kT}\right]$$

$$\sigma_{r\theta} = \sigma_{\theta r} = 0$$

$$\sigma_{rz} = \sigma_{zr} = 0$$

$$\sigma_{\theta z} = \sigma_{z\theta} = \frac{NkT}{J}\lambda_0^2 \zeta r \tag{19}$$

Investigation of Eq. (19) reveals that all the three normal stresses, σ_{rr}, $\sigma_{\theta\theta}$ and σ_{zz}, are significant influenced by both the elastic deformation and chemical field. The stress $\sigma_{\theta z}$ and $\sigma_{z\theta}$ due to the external torque T_0 are also implicit functions of the strain ζ and the chemical potential μ, where the dependence on chemical potential μ is included in the stretch λ_0, as explicitly expressed by Eq. (12).

Afterwards, the Equilibrium equations of Eq. (7) in cylinder coordinates can be written as

$$\frac{\partial \sigma_{rr}}{\partial r} + \frac{1}{r}\frac{\partial \sigma_{r\theta}}{\partial \theta} + \frac{\sigma_{rr} - \sigma_{\theta\theta}}{r} + \frac{\partial \sigma_{rz}}{\partial z} = 0$$

$$\frac{\partial \sigma_{\theta r}}{\partial r} + \frac{1}{r}\frac{\partial \sigma_{\theta\theta}}{\partial \theta} + \frac{\sigma_{r\theta} + \sigma_{\theta r}}{r} + \frac{\partial \sigma_{\theta z}}{\partial z} = 0$$

$$\frac{\partial \sigma_{zr}}{\partial r} + \frac{1}{r}\frac{\partial \sigma_{z\theta}}{\partial \theta} + \frac{\partial \sigma_{zz}}{\partial z} + \frac{\sigma_{zr}}{r} = 0 \tag{20}$$

of which the last two equations are automatically satisfied by Eq. (19), while the first equation can be reduced as the following ordinary derivative equation.

$$\frac{d\sigma_{rr}}{dr} + \frac{\sigma_{rr} - \sigma_{\theta\theta}}{r} = 0 \tag{21}$$

Using the chain rule, Eq. (21) can be further written as

$$\frac{d\sigma_{rr}}{dR} + \frac{\dot{r}}{r}(\sigma_{rr} - \sigma_{\theta\theta}) = 0 \tag{22}$$

and the derivatives of the terms of Eq. (19), the stress σ_{rr}, are obtained as

$$\frac{dJ}{dR} = \frac{d}{dR}\left(\frac{\dot{r}r}{R}\lambda_0\right) = \lambda_0\left(\ddot{r}\frac{r}{R} + \dot{r}\frac{\dot{r}R - r}{R^2}\right) = \lambda_0 \frac{\ddot{r}rR + \dot{r}(\dot{r}R - r)}{R^2}$$

$$\frac{d}{dR}\left[\frac{NkT}{J}(\dot{r}^2 - 1)\right] = -\frac{NkT}{J^2}\frac{dJ}{dR}(\dot{r}^2 - 1) + \frac{NkT}{J}(2\dot{r}\ddot{r})$$

$$\frac{d}{dR}\left[\ln\left(1 - \frac{1}{J}\right)\right] = \frac{1}{1 - \frac{1}{J}}\frac{1}{J^2}\frac{dJ}{dR} = \frac{1}{J(J-1)}\frac{dJ}{dR}$$

$$\frac{d}{dR}\left(\frac{1}{J}\right) = -\frac{1}{J^2}\frac{dJ}{dR}$$

$$\frac{d}{dR}\left(\frac{1}{J^2}\right) = -\frac{2}{J^3}\frac{dJ}{dR} \tag{23}$$

As a result, the force balance equation (22) can be presented explicitly as below.

$$\begin{aligned}&\left[-(\dot{r}^2 - 1) + \frac{1}{vN}\frac{2 - J}{J(J-1)} + 2\dot{r}^2\right]\ddot{r} + \left[-(\dot{r}^2 - 1)\right. \\ &\left. + \frac{1}{vN}\frac{2 - J}{J(J-1)}\right]\frac{\dot{r}}{r}\frac{(\dot{r}R - r)}{R} + \frac{\dot{r}^2}{r}\left[\dot{r}^2 - (r/R)^2 - \lambda_0^2\zeta^2 r^2\right] \\ &= 0\end{aligned} \tag{24}$$

where $J = \frac{\dot{r}r}{R}\lambda_0$. It is found that Eq. (24) is a nonlinear second-order ordinary differential equation of the current radial coordinate, $r(R)$, with respect to the original coordinate R. As mentioned above, the chemical potential μ is implicitly included in Eq. (24) through the stretch (12). Besides, the strain ζ is also included in Eq. (24), revealing that the coordinate r is influenced by both the strain ζ and the chemical potential μ, indicating a chemo-mechanical coupled effect on the deformation subject to extension and torsion.

In order to get solution to Eq. (24), boundary conditions need specified. By Eq. (19), the shear stresses $\sigma_{r\theta}$ and σ_{rz} are equal to 0, thus the boundary condition for the traction-free surface is given as

$$\sigma_{rr} = 0, \text{on } R = r_0 \tag{25}$$

Furthermore, to ensure that the deformation $\boldsymbol{F}$ is bounded, the following regularity is imposed as

$$r(R) \to 0, \text{if } R \to 0 \tag{26}$$

If the applied torque is denoted by T_0, it may be formulated by Eq. (19) with the stress $\sigma_{\theta z}$ as

$$T_0 = \int_D \sigma_{\theta z} \cdot r da = \int_0^{r_0} \sigma_{\theta z} \cdot 2\pi [r(R)]^2 dr \tag{27}$$

where D denotes the current cross section of the cylinder and da is a material element area after deformation. Since $dr = \dot{r} dR$ and the principal invariant $J = \frac{r}{R}\lambda_0$, the torque (27) then can be rewritten by Eq. (19), as

$$\begin{aligned} T_0 &= \int_0^{r_0} 2\pi [r(R)]^2 \sigma_{\theta z} dr = \int_0^{R_0} 2\pi [r(R)]^2 \sigma_{\theta z} \dot{r}(R) dR \\ &= \int_0^{R_0} 2\pi [r(R)]^2 \frac{NkT}{J} \lambda_0^2 \zeta r(R) \dot{r}(R) dR \end{aligned} \tag{28}$$

or inversely

$$\zeta = \frac{T_0}{\int_0^{R_0} 2\pi NkT \lambda_0 r^2 R dR} \tag{29}$$

Similarly, in order to maintain the axial stretch λ_0 unchanged with torsion, the axial extension F on any cross-section of the cylinder is required, and it may be obtained as

$$F = \int_D \sigma_{zz} da = \int_0^{r_0} \sigma_{zz} \cdot 2\pi r(R) dr \tag{30}$$

By Eq. (19) and $dr = \dot{r} dR$, the axial load (30) can be obtained as

$$\begin{aligned} F &= \int_0^{r_0} \sigma_{zz} \cdot 2\pi r(R) dr = \int_0^{R_0} \sigma_{zz} \cdot 2\pi r(R) \dot{r}(R) dR \\ &= \int_0^{R_0} 2\pi r \dot{r} \left\{ \frac{NkT}{J} \left(\lambda_0^2 - 1\right) + \frac{kT}{\nu} \left[\ln\left(1 - \frac{1}{J}\right) + \frac{1}{J} + \frac{\chi}{J^2} - \frac{\mu}{kT} \right] \right\} dR \end{aligned} \tag{31}$$

The above-formulated governing equations (24) and (28) to (31), along with the boundary conditions (26), (27) and fixed axial stretch, describe the finite deformation of extension and torsion for hydrogel cylinder at given chemical potential μ and torque T_0 in the continuum framework, together with axial loading F. The relation may thus be obtained among the stretch λ_0, torque T_0, strain ζ, radial position r and axial force F, where in the chemical potential μ and the microstructure parameters, such as crosslinking νN and Flory-Huggins parameter χ, are naturally incorporated. Furthermore, if the effect of the chemical potential is neglected, the large extension and torsion of an elastic cylinder, composed of homogeneous isotropic elastic material such as Blatz-Ko material can be recovered by reduction of the present nonlinear coupling theory (Kirkinis and Ogden, 2016; Polignone and Horgan, 1991).

In addition, as pointed out by previous works (Kirkinis and Ogden, 2016; Polignone and Horgan, 1991), appropriate axial traction needs to be supplied in order to maintain the finite deformation of soft materials subject to torque. It is observed that the axial force (31) is found and derived in this subsection. Furthermore, the sign of the axial load F reveals the positive or negative Poynting effect in such a way that negative loading F, or compression, indicates the typical Poynting effect, i.e., the cylinder tends to elongate when twisted (Poynting, 1909). Conversely, if the axial force F is positive, or extension, a negative Poynting effect may take place, i.e., the cylinder tends to shorten on twisting (Balbi et al., 2019). Additionally, the coupled effects of physical processes imposed by external loading and material parameter such as chemical potential μ, crosslinking νN and Flory-Huggins parameter χ, is numerically explored and discussed following section.

3. Numerical analysis: dynamic competition between mechanical and chemical loading

In this section, the combined torsion and extension of hydrogel is numerically investigated, for effects of loading and material parameters, such as torque T_0, Flory-Huggins parameter χ and degree of crosslinking νN. In particular, the typical nonlinear positive Poynting effect is discovered with a negative axial force F, where the cylinder radius tends to elongate. Also, the interplay between mechanical and chemical effects is discussed, revealing their dynamic competition through changes in network structure and chemical potential. In order to provide a more specific discussion, the normalized force $\widetilde{F}$ is introduced by dividing the force F by the shear modulus $NkT/2$ and area of cross section πR_0^2 as

$$\widetilde{F} = \frac{2F}{NkT \cdot \pi R_0^2} \tag{32}$$

Similarly, to normalize the torque, we relate the torque T_0 to the shear stress τ through the integral $T_0 = \int_0^{R_0} \tau \cdot 2\pi R dR$. Simplifying this with an average shear stress $\overline{\tau}$ to $T_0 = \overline{\tau} \int_0^{R_0} 2\pi R dR = \overline{\tau} \cdot 2\pi R_0^3/3$, we get the average shear stress as $\overline{\tau} = 3T_0/2\pi R_0^3$. This average shear stress is then normalized by the shear modulus $NkT/2$, resulting in the dimensionless or normalized torque $\widetilde{T}_0$ given by

$$\widetilde{T}_0 = \frac{3T_0}{NkT \cdot \pi R_0^3} \tag{33}$$

By Eqs (12), (24)–(26), (28) and (33), it is discovered that the torque T_0 is influenced by both the strain ζ and the chemical potential μ. Subsequently, the surface of normalized torque $\widetilde{T}_0$ with the strain ζ and the non-dimensionalized chemical potential $\widetilde{\mu}$ is shown in Fig. 3, to analyze the effect of chemo-mechanical coupling on the torque $\widetilde{T}_0$, where the cylinder radius $R_0 = 0.1m$, the Flory-Huggins parameter $\chi = 0.2$ and degree of crosslinking $\nu N = 10^{-3}$. It is found that the torque $\widetilde{T}_0$ is positively correlated with both the chemical potential $\widetilde{\mu}$ and strain ζ. The increase with strain aligns with general principles of mechanics, while the increase with chemical potential is attributed to a significant extension of the polymer chains, which leaves little room for further deformation, thereby requiring greater loading.

In details, Fig. 4 is plotted to show the variation of the normalized torque $\widetilde{T}_0$ with the non-dimensionalized chemical potential $\widetilde{\mu}$ for different strains $\zeta = 0.01, 0.02, 0.03, 0.04$ and 0.05. It is demonstrated that the normalized torque $\widetilde{T}_0$ increases with rising chemical potential,

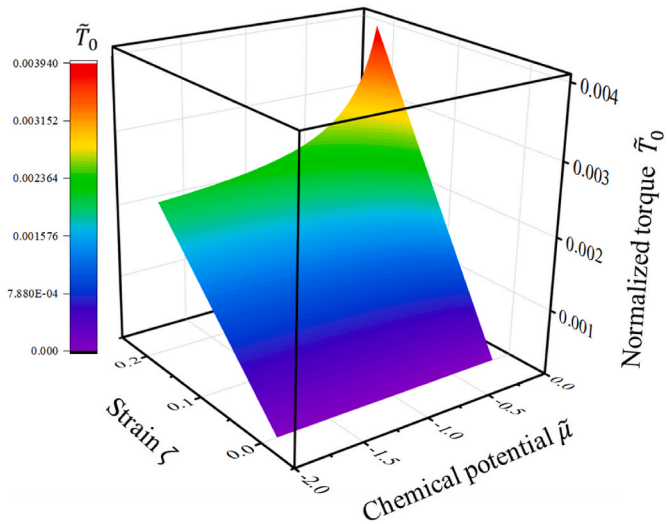

Fig. 3. The surface of normalized torque $\widetilde{T}_0$ with the strain ζ and the non-dimensionalized chemical potential $\widetilde{\mu}$, where $\chi = 0.2$ and $\nu N = 10^{-3}$.

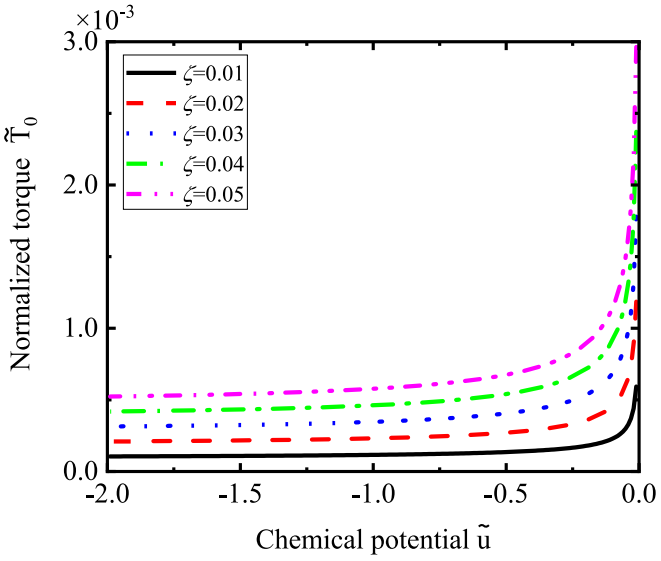

Fig. 4. Variation of the normalized torque $\widetilde{T}_0$ with the non-dimensionalized chemical potential $\widetilde{\mu}$ for different strains ζ, where $\chi = 0.2$ and $\nu N = 10^{-3}$.

which is consistent with the result of Fig. 3. As mentioned above, higher chemical potential reflects a greater solvent content, leading to more fully extended polymer chains. As a result, the hydrogel network becomes more resistant to twisting, requiring a higher torque to achieve the same strain. Besides, the torque $\widetilde{T}_0$ changes relatively slow when the chemical potential $\widetilde{\mu}$ is sufficiently low, whereas it increases rapidly as the chemical potential $\widetilde{\mu}$ approaches zero, reflecting an increasing influence of the chemical field at high solvent content. Furthermore, a higher strain ζ corresponds to a higher torque $\widetilde{T}_0$ for fixed chemical potential $\widetilde{\mu}$.

In addition, the intrinsic Flory-Huggins parameter χ also have significant influence on the normalized torque $\widetilde{T}_0$ through tuning the hydrophilicity of hydrogel, thereby affecting the stretch λ_0. Fig. 5 is then plotted by Eqs (12) and (28) to show the variation of the normalized torque $\widetilde{T}_0$ with the Flory-Huggins parameter χ subject to different chemical potentials $\widetilde{\mu} = -0.8, -0.7, -0.6, -0.5, -0.4$, where the strain $\zeta = 0.01$ and $\nu N = 10^{-3}$. It is observed in Fig. 5 that the torque $\widetilde{T}_0$ decrease with the increase of Flory-Huggins parameter χ. This is attributed to fact that an increase in the Flory-Huggins parameter χ reduces the hydrophilicity of hydrogel, leading to a decrease in the stretch λ_0, consequently, a lower solvent content. By the conclusions drawn from Fig. 4, this results in a lower torque $\widetilde{T}_0$. This relationship is further supported by the formulations in Eqs (12) and (28) and Fig. 2(b), where the stretch λ_0 consistently decreases as the Flory-Huggins parameter χ increases. Therefore, the torque $\widetilde{T}_0$ is monotonically and inversely proportional to the Flory-Huggins parameter χ, since it is positively correlated with the stretch λ_0 and solvent content. In addition, if the Flory-Huggins parameter χ is fixed, a higher chemical potential $\widetilde{\mu}$ corresponds to a larger torque $\widetilde{T}_0$ subject to chemo-mechanical coupling effect, which is consistent with the result of Fig. 4.

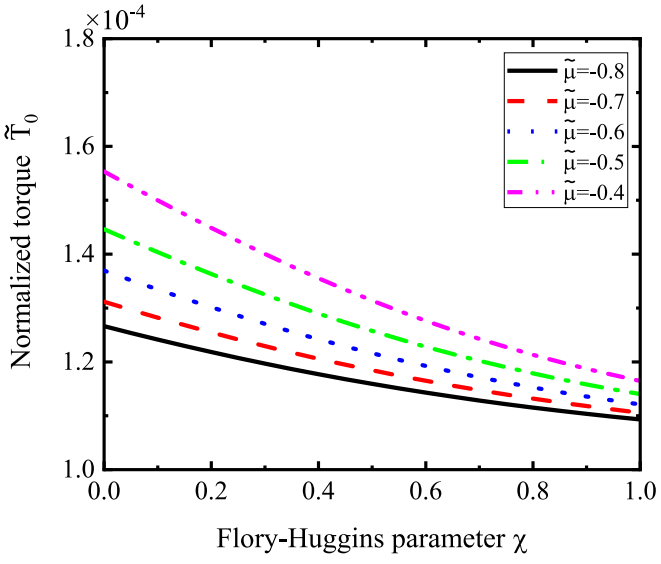

Fig. 5. Variation of the normalized torque $\widetilde{T}_0$ with the Flory-Huggins parameter χ subject to the different non-dimensionalized chemical potential $\widetilde{\mu}$, and $\nu N = 10^{-3}$.

Furthermore, as well known and also noticed in Fig. 2(c), the crosslinking νN is a critical internal structural parameter that directly affects the macroscopic deformation of the hydrogel. When analyzing the effect of crosslinking νN, it is important to note that normalizing the force and torque with $NkT/2$ becomes unreasonable since the parameter N is now a variable. Besides, normalizing these quantities with a fixed crosslinking parameter N_0 would also be inappropriate. Therefore, in the following discussions of Figs. 6 and 10 regarding the effect of crosslinking νN, both the normalized torque $T_0/\frac{2}{3}\pi R_0^3$ and the normalized force $F/\pi R_0^2$ are expressed in unit of Pascals, without normalization by the shear modulus. It should also be noted that, similar as the effect of Flory-Huggins parameter χ, the contribution of the crosslinking νN consists of two parts as demonstrated by Eq (28), of which one is the elasticity of the structure itself ($\nu NKT/\nu$) and the other is the indirect contribution by the stretch (12). By Eqs (12) and (28), Fig. 6 is plotted to show the variation of the normalized torque $3T_0/2\pi R_0^3$ with the crosslinking νN subject to different chemical potentials $\widetilde{\mu} = -0.8, -0.7, -0.6, -0.5, -0.4$, where the strain $\zeta = 0.01$ and Flory-Huggins parameter $\chi = 0.2$. With the increase of the crosslinking νN, the hydrogel becomes stiffer, leading to an increase in its stretch λ_0 as shown in Fig. 2(c), and a larger torque $3T_0/2\pi R_0^3$ is then required. Consequently, the torque $3T_0/2\pi R_0^3$ is positively correlated with the crosslinking νN as shown in Fig. 6. In addition, for a given chemical potential $\widetilde{\mu}$, the change in the slope of curve is relatively modest if the crosslinking

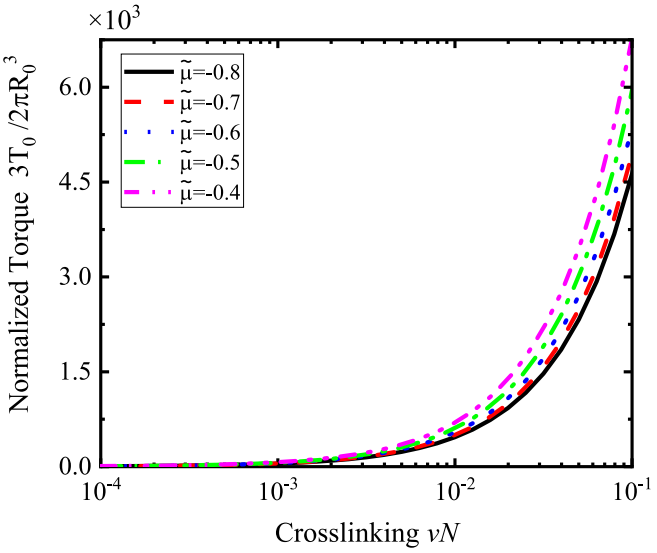

Fig. 6. Variation of the normalized torque $3T_0/2\pi R_0^3$ with the crosslinking νN subject to the different non-dimensionalized chemical potential $\widetilde{\mu}$, and $\chi = 0.2$.

νN is less than $\sim 10^{-2}$, while the curve becomes steeper with rapidly increasing torque when the crosslinking νN increases from $\sim 10^{-2}$ to 10^{-1}.

Similarly, by Eqs (12), (31) and (32), it is discovered that the normalized axial force $\widetilde{F}$ is influenced by both the strain ζ and the chemical potential μ. Subsequently, the surface of normalized axial force $\widetilde{F}$ with the strain ζ and the non-dimensionalized chemical potential $\widetilde{\mu}$ is shown in Fig. 7(a), to analyze the effect of chemo-mechanical coupling on the axial force $\widetilde{F}$, where $\chi = 0.2$ and $\nu N = 10^{-3}$. Generally, Poynting effect describes the phenomenon that the specimen tends to elongation upon twisting. This case happens when no axial force is present. An equivalent expression of this effect is that a compressive force along the axial direction is required to maintain the axial length upon twisting, which is the approach we adopt in the present paper. By Fig. 7(a), it is found that the axial force $\widetilde{F}$ is negative to maintain the stretch, revealing a positive Poynting effect. This may be understood by Fig. 7(b) that shows the surface of radial position r with the strain ζ and initial radial coordinate R, in such a way that radial elongation (24) of the hydrogel cylinder requires an axial shortening to assure the incompressibility condition. Fig. 8 then shows the variation of the normalized axial force $\widetilde{F}$ with the non-dimensionalized chemical potential $\widetilde{\mu}$ with different strains

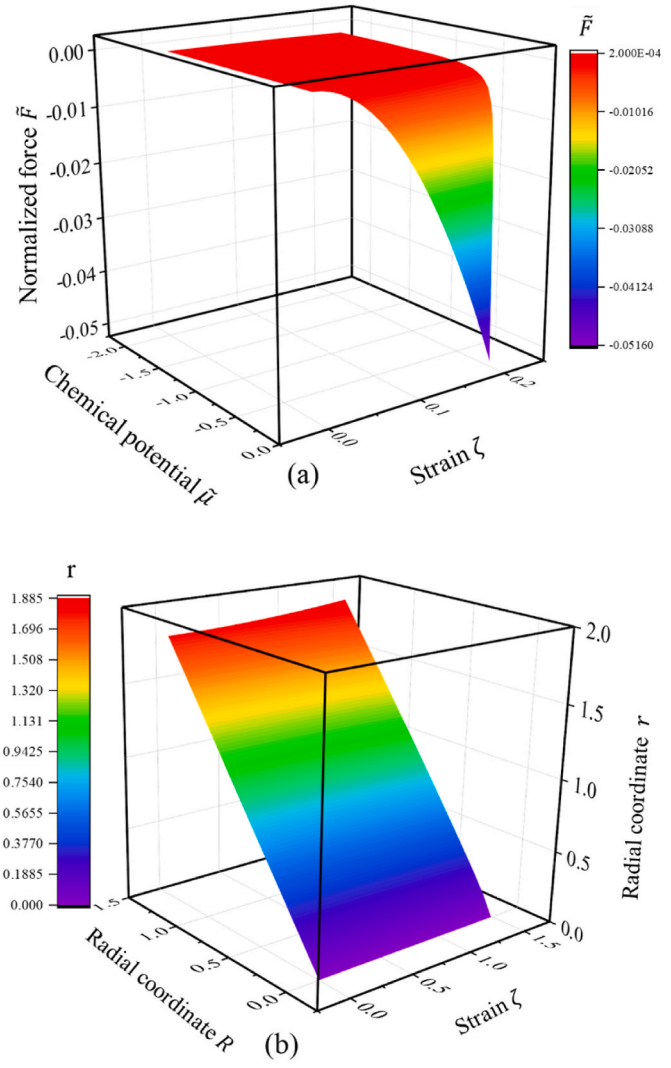

Fig. 7. The surface of normalized axial force $\widetilde{F}$ with the strain ζ and the non-dimensionalized chemical potential $\widetilde{\mu}$ (a), and the surface radial coordinate r with the strain ζ and initial radial coordinate R (b), where $\chi = 0.2$ and $\nu N = 10^{-3}$.

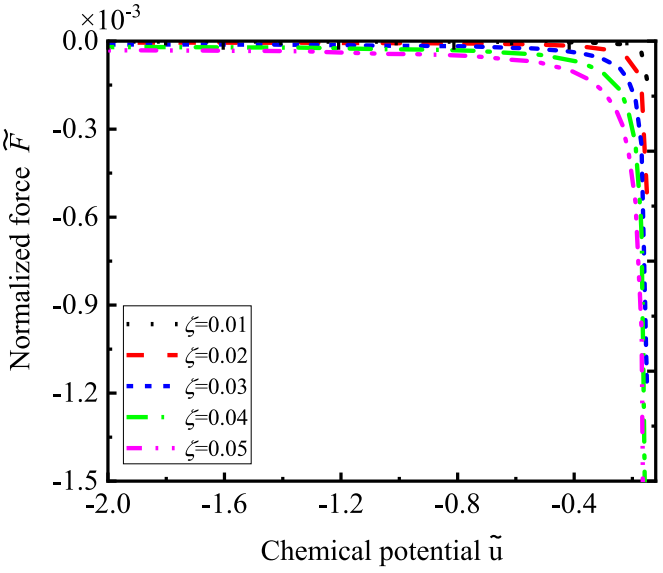

Fig. 8. Variation of the normalized axial force $\widetilde{F}$ with the non-dimensionalized chemical potential $\widetilde{\mu}$ for different strains ζ, where $\chi = 0.2$ and $\nu N = 10^{-3}$.

$\zeta = 0.01$, 0.02, 0.03, 0.04 and 0.05, where $\chi = 0.2$, $\nu N = 10^{-3}$. It is demonstrated that an increase in the chemical potential $\widetilde{\mu}$ can lead to a rise in the axial force $\widetilde{F}$. This result may be attributed to two aspects. Firstly, an increase in chemical potential results in larger solvent content at equilibrium, leaving little room for further deformation and increasing resistance. As a result, a larger force $\widetilde{F}$ is required as chemical potential rises. Secondly, from a deformation perspective, twisting may reduce the internal chemical potential, encouraging the hydrogel to absorb more solvent, which leads to both radial and axial expansion. While in this scenario where the axial deformation is preserved during twist, an addition compressive axial force is necessary. As a general principle, an increase in chemical potential leads to greater solvent content, resulting in more significant dilation and, consequently, a larger axial force is required. Furthermore, for a fixed chemical potential $\widetilde{\mu}$, an increase in the applied strain ζ on the hydrogel also corresponds to a higher axial force $\widetilde{F}$, which is consistent with the trends observed in Fig. 7(a). All of these results are a manifestation of the competition between mechanical interaction of strain ζ and solvent diffusion up to equilibrium with chemical potential $\widetilde{\mu}$.

Furthermore, Figs. 9 and 10 are plotted by Eqs ((12), (24), (31) and (32) to show the variations of the normalized force $\widetilde{F}$ with the Flory-Huggins parameter χ and normalized axial force $F/\pi R_0^2$ with crosslinking νN respectively, subject to different chemical potentials $\widetilde{\mu} = -0.8, -0.7, -0.6, -0.5, -0.4$, where the strain $\zeta = 0.01$, $\nu N = 10^{-3}$ in Fig. 9 and $\chi = 0.2$ in Fig. 10. It can be seen from Fig. 9 that the normalized axial force $\widetilde{F}$ is inversely proportional to the Flory-Huggins parameter χ. An increase in the Flory-Huggins parameter χ reduces the hydrophilicity of the hydrogel, leading to a decrease in the stretch λ_0 and, consequently, a lower solvent content. As concluded in Figs. 7 and 8, the decrease in solvent content results in a lower force $\widetilde{F}$. In addition, as shown in Fig. 10, a larger axial force $F/\pi R_0^2$ is required for increasing crosslinking νN, as the hydrogel becomes stiffer with higher crosslinking. Furthermore, both Figs. 9 and 10 reveal that an increase in the chemical potential $\widetilde{\mu}$ can lead to a rise in the axial force for a fixed Flory-Huggins parameter χ or crosslinking νN, which is the same as in Fig. 8. To sum up, the variation of physical parameters such as the Flory-Huggins parameter and crosslinking plays an important role in the dynamic competition between mechanical and chemical effects, which provides guidelines for the design and application of hydrogels.

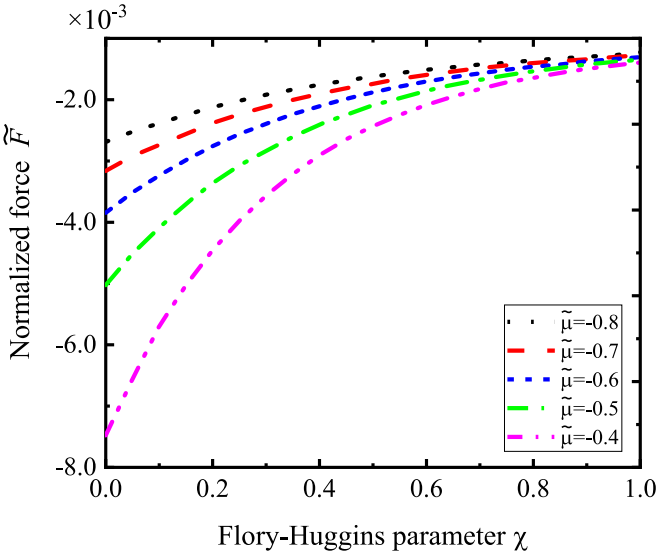

Fig. 9. Variation of the normalized axial force $\widetilde{F}$ with the Flory-Huggins parameter χ subject to the different non-dimensionalized chemical potential $\widetilde{\mu}$, and $\nu N = 10^{-3}$.

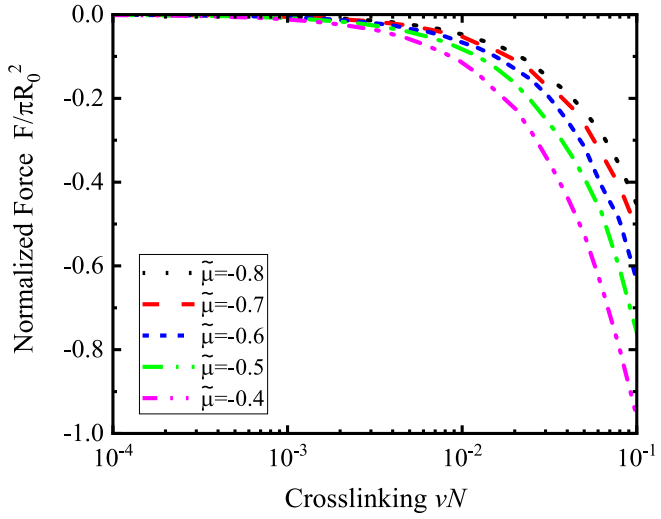

Fig. 10. Variation of the normalized axial force $F/\pi R_0^2$ with the crosslinking νN subject to the different non-dimensionalized chemical potential $\widetilde{\mu}$, and $\chi = 0.2$.

4. Conclusions

Based on the framework of continuum mechanics, a detailed theoretical analysis and numerical investigation of the combined extension and torsion of hydrogel cylinder is presented under chemo-mechanical coupled loading, where the chemical field is coupled with finite deformation through incorporating the incompressibility constraints via Legendre transformation. The significant observations and conclusions are summarized below. Firstly, a simplified, closed-form analytical model is derived to accurately describe the chemo-mechanical coupled response of hydrogel, considering the effects of external load, chemical potential, and microphysical parameters such as the degree of crosslinking and Flory-Huggins interaction. This provides a robust theoretical foundation for in-depth understanding of the complex deformation mechanisms in hydrogel. Secondly, the impacts of free swelling and microscopic diffusion of hydrogels are systematically analyzed at equilibrium state. The influences of various parameters, such as the chemical potential and crosslinking, on the macroscopic deformation and fundamental properties are revealed, offering valuable theoretical guidance for designing high-performance hydrogel. Furthermore, the classic Poynting effect, where hydrogel cylinder tends to elongate on twisting, is discovered and explained. The inhomogeneous deformation, induced by torsion, along the radial direction is demonstrated, shedding more light on the complex deformation behavior of hydrogel. Finally, the dynamic competition between external loads and solvent environment is explored at equilibrium state, establishing direct connections between internal microscopic parameters and macroscopic deformation. The torque is positively correlated with both the chemical potential and strain, and an increase in the chemical potential can lead to a rise in the axial force. In summary, the analysis of complex loading and boundary condition will be of universal interest to the mechanics community. The theoretical results presented in this paper may provide predictions and guidance for the mechanical analysis and engineering applications of hydrogel cylinder subject to extension and torsion in a solvent.

CRediT authorship contribution statement

Chengxiang Zheng: Writing – review & editing, Writing – original draft, Visualization, Investigation, Data curation. **Minghui Hu:** Methodology, Data curation. **Wenyi Wang:** Methodology, Data curation. **Qian Li:** Supervision, Funding acquisition. **Pasquale Ciarletta:** Formal analysis, Conceptualization. **Tao Wu:** Writing – original draft, Funding acquisition, Conceptualization. **Zichen Deng:** Writing – review & editing, Supervision, Funding acquisition.

Declaration of competing interest

The authors declare that they have no known competing financial interests or personal relationships that could have appeared to influence the work reported in this paper.

Data availability

No data was used for the research described in the article.

Acknowledgements

This work is supported by the National Natural Science Foundation of China (Grants No. 12232015), Natural Science Basic Research Plan in Shaanxi Province of China (Grants No. 2023-JC-QN0037), Funding of the China Scholarship Council (CSC), and the Open Foundation of the Guangdong Provincial Key Laboratory of Electronic Information Products Reliability Technology.

References

Balbi, V., Trotta, A., Destrade, M., Ni Annaidh, A., 2019. Poynting effect of brain matter in torsion. Soft Matter 15, 5147–5153.
Chester, S.A., Anand, L., 2010. A coupled theory of fluid permeation and large deformations for elastomeric materials. J. Mech. Phys. Solid. 58, 1879–1906.
Demiray, H., 1972. A note on the elasticity of soft biological tissues. J. Biomech. 5, 309–311.
Dolbow, J., Fried, E., Ji, H., 2004. Chemically induced swelling of hydrogels. J. Mech. Phys. Solid. 52, 51–84.
Duda, F.P., Ciarbonetti, A., Toro, S., Huespe, A.E., 2018. A phase-field model for solute-assisted brittle fracture in elastic-plastic solids. Int. J. Plast. 102, 16–40.
Duda, F.P., Souza, A.C., Fried, E., 2010. A theory for species migration in a finitely strained solid with application to polymer network swelling. J. Mech. Phys. Solid. 58, 515–529.
Flory, P.J., Rehner, J., 1943. Statistical mechanics of cross-linked polymer networks I Rubberlike elasticity. J. Chem. Phys. 11, 512–520.
Fung, Y., 1967. Elasticity of Soft Tissues in Simple Elongation, vol. 213, pp. 1532–1544.
Hao, Y., Zhang, S., Fang, B., Sun, F., Liu, H., Li, H., 2022. A review of smart materials for the boost of soft actuators, soft sensors, and robotics applications. Chin. J. Mech. Eng. 35, 1–16.
Hong, W., Liu, Z., Suo, Z., 2009. Inhomogeneous swelling of a gel in equilibrium with a solvent and mechanical load. Int. J. Solid Struct. 46, 3282–3289.

Hong, W., Zhao, X., Zhou, J., Suo, Z., 2008. A theory of coupled diffusion and large deformation in polymeric gels. J. Mech. Phys. Solid. 56, 1779–1793.
Horgan, C.O., Murphy, J.G., 2015. Reverse poynting effects in the torsion of soft biomaterials. J. Elasticity 118, 127–140.
Horgan, C.O., Smayda, M.G., 2012. The importance of the second strain invariant in the constitutive modeling of elastomers and soft biomaterials. Mech. Mater. 51, 43–52.
Huggins, M.L., 1941. Solutions of long chain compounds. J. Chem. Phys. 9, 440.
Ji, H.D., Mourad, H., Fried, E., Dolbow, J., 2006. Kinetics of thermally induced swelling of hydrogels. Int. J. Solid Struct. 43, 1878–1907.
Kanner, L.M., Horgan, C.O., 2008a. Inhomogeneous shearing of strain-stiffening rubber-like hollow circular cylinders. Int. J. Solid Struct. 45, 5464–5482.
Kanner, L.M., Horgan, C.O., 2008b. On extension and torsion of strain-stiffening rubber-like elastic circular cylinders. J. Elasticity 93, 39–61.
Kirkinis, E., Ogden, R.W., 2016. On extension and torsion of a compressible elastic circular cylinder. Math. Mech. Solid 7, 373–392.
Li, H., Luo, R., Birgersson, E., Lam, K.Y., 2007. Modeling of multiphase smart hydrogels responding to pH and electric voltage coupled stimuli. J. Appl. Phys. 101.
Li, H., Luo, R., Birgersson, E., Lam, K.Y., 2009. A chemo-electro-mechanical model for simulation of responsive deformation of glucose-sensitive hydrogels with the effect of enzyme catalysis. J. Mech. Phys. Solid. 57, 369–382.
Li, H., Wang, X., Yan, G., Lam, K.Y., Cheng, S., Zou, T., Zhuo, R., 2005. A novel multiphysic model for simulation of swelling equilibrium of ionized thermal-stimulus responsive hydrogels. Chem. Phys. 309, 201–208.
Li, S., Cong, Y., Fu, J., 2021. Tissue adhesive hydrogel bioelectronics. J. Mater. Chem. B 9, 4423–4443.
Li, W., Guan, Q., Li, M., Saiz, E., Hou, X., 2023. Nature-inspired strategies for the synthesis of hydrogel actuators and their applications. Prog. Polym. Sci. 140.
Liu, C., Du, Y., Li, K., Zhang, Y., Han, Z., Zhang, Y., Qu, S., Lü, C., 2022. Geometrical incompatibility guides pattern selection in growing bilayer tubes. J. Mech. Phys. Solid. 169.
Ogden, R., 1997. Non-linear Elastic Deformations. Ellis Horwood, Chichester, 1984. Dover reissue.
Polignone, D.A., Horgan, C.O., 1991. Pure torsion of compressible non-linearly elastic circular cylinders. Q. Appl. Math. 49, 591–607.
Poynting, J.H., 1909. On pressure perpendicular to the shear planes in finite pure shears, and on the lengthening of loaded wires when twisted. Proc. R. Soc. Lond. - Ser. A Contain. Pap. a Math. Phys. Character 82, 546–559.
Poynting, J.H., 1912. On the changes in the Dimensions of a steel wire when twisted, and on the pressure of distortional waves in steel. Proc. R. Soc. Lond. - Ser. A Contain. Pap. a Math. Phys. Character 86, 534–561.
Rivlin, R.S., 1949. Large elastic deformations of isotropic materials VI. Further results in the theory of torsion, shear and flexure. J Philosophical Transactions of the Royal Society of London. Series A, Mathematical Physical Sciences 242, 173–195.
Rivlin, R.S., Rideal, E.K., 1948. Large elastic deformations of isotropic materials IV. further developments of the general theory 241, 379–397.
Su, Y., Conroy Broderick, H., Chen, W., Destrade, M., 2018. Wrinkles in soft dielectric plates. J. Mech. Phys. Solid. 119, 298–318.
Wang, D., Wu, M.S., 2014. Poynting and axial force–twist effects in nonlinear elastic mono- and bi-layered cylinders: torsion, axial and combined loadings. Int. J. Solid Struct. 51, 1003–1019.
Wang, T., Yang, Y., Fu, C., Liu, F., Wang, K., Xu, F., 2020. Wrinkling and smoothing of a soft shell. J. Mech. Phys. Solid. 134.
Wu, M.S., Kirchner, H.O.K., 2010. Nonlinear elasticity modeling of biogels. J. Mech. Phys. Solid. 58, 300–310.
Wu, M.S., Wang, D., 2015. Nonlinear effects in composite cylinders: relations and dependence on inhomogeneities. Int. J. Eng. Sci. 90, 27–43.
Wu, T., Zheng, C., Deng, Z., 2022. Second-order elasticity of polymeric hydrogels with chemically coupled effects. Int. J. Mech. Sci. 230, 107539.
Zheng, C., Wu, T., Deng, Z., 2022. Torsion of hydrogel cylinder with a chemo-mechanical coupled nonlinear elastic theory. Int. J. Solid Struct. 248, 111670.